E-ISSN: 3123-2507
DOI: https://doi.org/10.64803/cessmuds.v1.90

A Numerical Study on the Effect of Structured Multizone Meshing on Air-Foil Aerodynamics at Low Angles of Attack

Andri Ramadhan[1*], Maharani Putri[2]

[1]Department of Energy and Refrigerating Air-Conditioning Engineering, National Taipei University of Technology, Taipei, 106344, Taiwan
[1]Department of Mechanical Engineering, Universitas Al-Azhar, Medan 20142, Indonesia
[2]Department of Electrical Engineering, National Taiwan University of Science and Technology, Taipei, 106335, Taiwan
[2]Department of Electrical Engineering, Politeknik Negeri Medan, Medan, North Sumatra 20155, Indonesia
Email: [1*]t113459402@ntut.org.tw, [2]maharaniputri@polmed.ac.id
*E-mail Corresponding Author: t113459402@ntut.org.tw

Abstract

This study presents a numerical analysis of airfoil aerodynamic characteristics at low angles of attack using a structured multizone meshing approach. The computational model was developed in ANSYS Workbench, with simulations conducted using ANSYS Fluent on a two-dimensional airfoil enclosed within a far-field domain. The mesh configuration consists of approximately 540,000 elements and 541,000 nodes, achieving a maximum skewness below 0.26, which indicates high mesh quality and numerical stability. Steady-state simulations were performed for angles of attack of −5°, 0°, 5°, and 10° to evaluate lift and drag behaviour, as well as pressure and velocity distributions around the airfoil surface. The numerical results show a consistent increase in lift coefficient with increasing angle of attack, accompanied by a corresponding rise in drag coefficient. At moderate angles of attack, particularly around 5°, the airfoil demonstrates an optimal aerodynamic performance with a favourable lift-to-drag ratio. These findings highlight the capability of structured multizone meshing to accurately capture key aerodynamic trends while maintaining computational efficiency. The results confirm that this meshing strategy is suitable for preliminary aerodynamic analysis and early-stage design of airfoil-based applications, such as small-scale wind turbine blades operating under low to moderate inflow conditions.

Keywords*: Air-foil Aerodynamics; CFD; MultiZone mesh; Angle of Attack; Wind Turbine.*

I. INTRODUCTION

Airfoil aerodynamic performance is of critical importance to the efficiency of wind turbines, propellers, and various turbomachinery components. For small-scale wind turbines, which frequently operate within low to moderate Reynolds number ranges and under fluctuating wind conditions, it is imperative to develop a thorough understanding of airfoil behaviour at low angles of attack (W. Du *et al.*,2022) . The relationship between angle of attack, lift, and drag directly affects the torque and power that can be extracted from the wind (K. S. Bhole, et al, 2023) ,(J.P.Narayanan, etal, 2025).

Computational Fluid Dynamics (CFD) has become an indispensable tool for predicting airfoil characteristics, thus obviating the need for extensive wind tunnel experimentation (S. M. T. Islam, et al, 2025). The employment of appropriate numerical methods, mesh strategies, and boundary conditions facilitates the detailed visualisation of pressure and velocity fields, in addition to the estimation of lift and drag forces for varying operating conditions (V. Filipe, etal, 2025).

In this study, a numerical investigation was conducted utilising the ANSYS Workbench (comprising the SpaceClaim and Meshing modules) and Fluent to analyse the aerodynamic response of an airfoil at four selected angles of attack: Specifically, the values considered were -5°, 0°, 5°, and 10° (B. Wei, etal 2024). The following aspects are of particular relevance:

1. The construction of a high-quality, structured MultiZone mesh surrounding the airfoil is imperative.
2. The evaluation of mesh quality metrics is undertaken to ensure numerical reliability.
3. The present study investigates how changes in angle of attack influence aerodynamic trends, including lift, drag, and flow field patterns.

The present study is intended as an initial step towards more comprehensive wind turbine blade investigations, where the present airfoil can be considered as a section of a turbine blade.

II. RESEARCH METHODOLOGY

a. Geometry and Computational Domain

The airfoil geometry, designated as 'Plane airfoil Original 200' within the project, is imported into ANSYS SpaceClaim from an external CAD file. The model is treated as a surface body with zero thickness and is embedded in a rectangular far-field domain (M. A. Aziz, etal, 2025). The global bounding box of the geometry is approximately 7 m

in the streamwise (X) direction and 5 m in the normal (Y) direction. The far-field boundaries (inlet, outlet, and upper/lower walls) are located several chord lengths away from the airfoil, with the objective of minimising blockage and confinement effects. The following named selections have been created for:

1. The upstream boundary is defined as the inlet.
2. The downstream boundary is defined as the outlet.
3. The upper and lower far-field boundaries of Wall's are as follows:

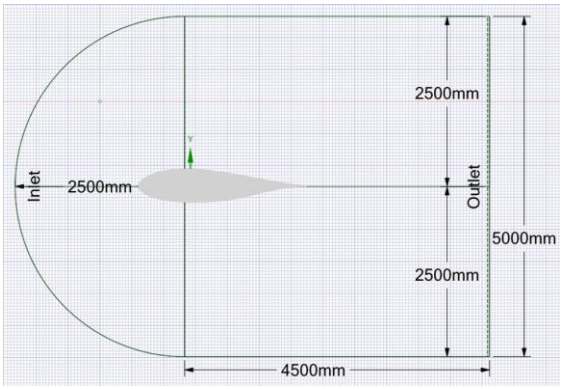

Figure 1. Airfoil and computational domain

The airfoil is defined as the surface of an aircraft wing that is employed to provide traction on a slippery surface (J. P. Narayanan, et al,2025) .

This configuration facilitates the unambiguous allocation of boundary conditions in Fluent for all simulated angles of attack.

Table 1. Summary of geometry and domain

Airfoil characteristics	DU 06-W-200
Chord length	200 mm
Domain length	7000 mm
Domain height	5000 mm
Type	2D airfoil

b. Mesh Generation and Quality

Mesh generation is performed in ANSYS Meshing with CFD physics preference and Fluent solver preference. A MultiZone Quad/Tri method is applied to the airfoil domain, enabling a structured or semi-structured grid with quadrilateral elements as the primary cell type around the airfoil. Edge sizing controls are imposed on several edges to refine the mesh near the airfoil and along the wake, with the number of divisions on selected edges reaching up to 350 in order to capture boundary-layer and wake gradients (Y.T. Lee, K. Ramesh, and A. Gopalarathnam, ,2025).

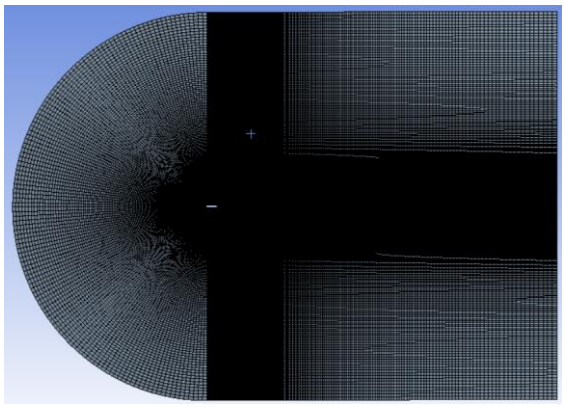

Figure 2. Mesh around DU 06-W200 airfoil

The final mesh contains approximately 541,593 nodes and 540,050 elements. Mesh quality is evaluated using skewness as the primary metric, yielding:

1. Minimum skewness ≈ 1.4×10^{-10}
2. Maximum skewness ≈ 0.259
3. Average skewness ≈ 0.038

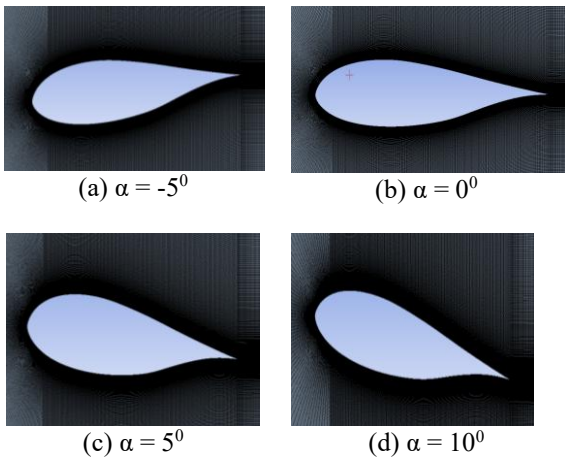

(a) $\alpha = -5^0$ (b) $\alpha = 0^0$

(c) $\alpha = 5^0$ (d) $\alpha = 10^0$

Figure 3. Close-up view of mesh near the airfoil surface

These values indicate a high-quality mesh, well below typical skewness thresholds for reliable CFD simulations.

Table 2. Mesh parameters and quality indicators

Description	Value
Elements	Quad/Tri
Number of nodes	538083
Number of elements	536550
Minimum element size	0.0027
Maximum element size	0.99947
Average element size	0.46664

Automatic inflation is set to a small number of layers (maximum 2) to resolve near-wall behavior

E-ISSN: 3123-2507
DOI: https://doi.org/10.64803/cessmuds.v1.90

while keeping the mesh size manageable for conference-level computation. If higher fidelity in boundary-layer resolution is required, additional inflation layers and y^+ control may be introduced in future work.

c. Boundary Conditions and Solver Settings

The simulations are carried out using ANSYS Fluent with the following general assumptions:

1. Incompressible, steady-state viscous flow,
2. Two-dimensional flow around the airfoil (modeled via a surface in a thin 3D domain),
3. No-slip boundary condition on the airfoil surface,
4. Prescribed velocity at the inlet and static pressure at the outlet,
5. Symmetry or far-field type treatment on the upper and lower boundaries.

Table 3. Boundary conditions and named selections

Boundary name	Type	Description
Inlet	Velocity inlet	Component, Absolute, V = 10 m/s, Turbulent Intensity = 10%
Outlet	Pressure outlet	Gauge pressure = 0 Pa, Turbulent Intensity = 10%
Wall_top	Symmetry/far-field	Upper boundary
Wall_bottom	Symmetry/far-field	Lower boundary
Airfoil	Stationary Wall/No Slip	DU 06-W200 surface
Density	Air	1.225 kg/m^3
Dynamic Viscosity	Air	0.000017894 kg/m-s

The angle of attack is imposed by rotating the airfoil geometry or by adjusting the direction of the incoming velocity vector to −5°, 0°, 5°, and 10°. For each case, the solution is iterated until the residuals of continuity and momentum reach acceptable convergence criteria and the lift and drag coefficients have stabilized.

III. RESULTS AND DISCUSSION

a. Flow Field Characteristics

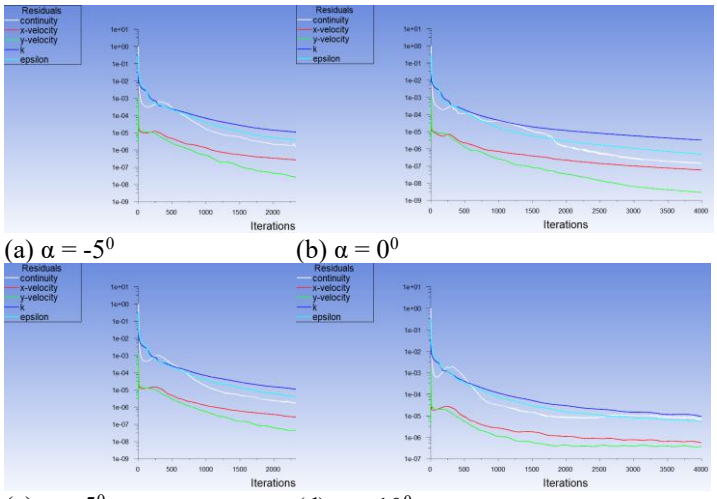

(a) α = -5^0 (b) α = 0^0

(c) α = 5^0 (d) α = 10^0

Figure 4. Residual convergence showing the continuity, x-velocity, y-velocity, turbulent kinetic energy k, and dissipation rate ε as functions of the iteration count.

Figure 4 illustrates the convergence behaviour of the governing equations for the 0° angle-of-attack simulation. Over 4,000 iterations, all residuals decrease monotonically by several orders of magnitude. The continuity residual drops from an initial value of 1.0 to about 1.45×10^{-7}, while the x- and y-momentum residuals are reduced from the order of 10^{-6} to 5.94×10^{-8} and 2.88×10^{-9}, respectively. The residuals of the turbulent kinetic energy $k$and its dissipation rate εdecrease from 1.09×10^{-1} and 3.18×10^{-1} to approximately 3.26×10^{-6} and 4.91×10^{-7}. This substantial reduction confirms that a well-converged steady-state solution is obtained. The simulations at −5°, 5°, and 10° exhibit a similar residual decay pattern, indicating consistent numerical convergence across all four operating conditions.

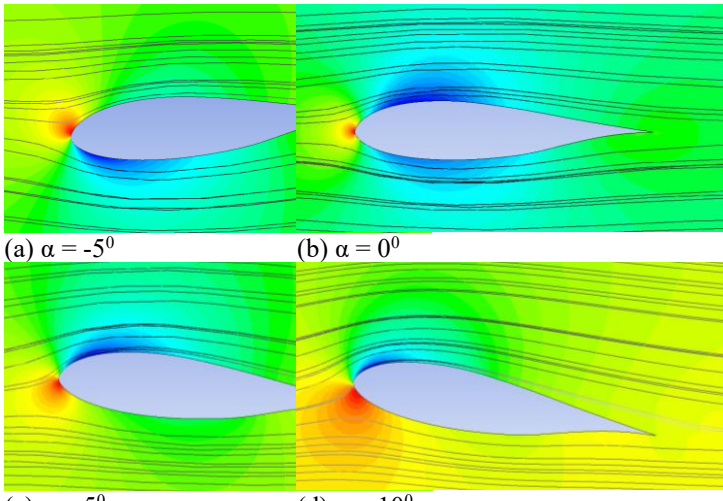

(a) α = -5^0 (b) α = 0^0

(c) α = 5^0 (d) α = 10^0

Figure 5. Flow pattern over plane airfoil (DU 06 W 200) observed by different angle of attack.

Figures 5. present the velocity magnitude contours and streamlines around the airfoil for the four simulated angles of attack. At −5°, the flow remains largely attached, but the effective camber is reduced, resulting in a slightly negative or low positive lift. The pressure difference between the suction and pressure sides is relatively small.

At 0°, the airfoil produces modest lift as the pressure on the upper surface becomes slightly lower than on the lower surface. The flow still appears fully attached, with a thin wake region downstream.

At 5°, a stronger pressure gradient develops, yielding higher lift. The contour and streamline plots show increased acceleration over the suction side and a somewhat thicker wake region, reflecting higher drag. This condition typically represents a favorable operating point where the lift-to-drag ratio is relatively high.

At 10°, the suction peak further intensifies and the boundary layer on the upper surface becomes more prone to separation. Depending on the Reynolds number and the airfoil shape, incipient or partial separation may be observed near the trailing edge. The wake region grows thicker, indicating a noticeable increase in drag.

Table 4. Residual levels of selected variables for each angle-of-attack case.

Angle of attack, α (deg)	Continuity residual	k residual	ε residual
−5	4.60×10^{-7}	3.90×10^{-6}	8.75×10^{-7}
0	1.45×10^{-7}	3.26×10^{-6}	4.91×10^{-7}
5	8.59×10^{-7}	$\approx 3.00 \times 10^{-6}$	5.20×10^{-7}
10	7.05×10^{-6}	$\approx 9.36 \times 10^{-6}$	5.46×10^{-6}

These qualitative trends are consistent with general airfoil aerodynamics and support the use of the present CFD model for preliminary analyses.

b. Lift and Drag Trends with Angle of Attack

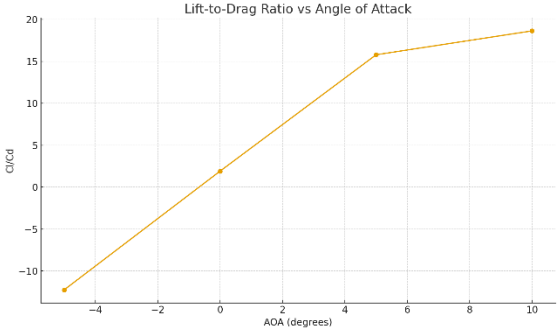

Figure 7. Lift-to-drag ratio C_l/C_d of the DU 06-W200 airfoil as a function of angle of attack.

The simulation results, summarized in the graphs for −5°, 0°, 5°, and 10°, show the expected variation of lift and drag with angle of attack:

1. Lift coefficient (C_l) increases approximately linearly between −5° and 10°,
2. Drag coefficient (C_d) also increases with angle of attack, due to stronger pressure drag and possibly early separation at higher angles,
3. The lift-to-drag ratio (C_l/C_d) reaches its maximum at a moderate angle (typically around 5°), which is desirable for energy extraction in wind turbine applications.

Table 5. Converged aerodynamic coefficients of the DU 06-W200 airfoil

Angle of attack, α (deg)	C_l	C_d	C_l/C_d
−5	−0.4221	0.0344	−12.25
0	0.0587	0.0306	1.92
5	0.5493	0.0348	15.80
10	0.9453	0.0507	18.65

Such presentation makes it clear how sensitive the airfoil performance is to small variations in operating angle.

c. Implications for Wind Turbine Blade Sections

For small-scale wind turbines, blade sections often operate within a relatively narrow range of angles of attack, depending on wind speed, tip-speed ratio, and pitch control. The present results indicate that:

1. Negative angles (−5°) are unfavorable for energy capture due to low lift.
2. Zero angle can be used but does not fully exploit the airfoil's lift potential.
3. A moderate positive angle (5°) offers a good balance between high lift and acceptable drag, making it a promising candidate for nominal operating conditions.
4. Higher angles (10° and above) may provide more lift but at the cost of rapidly increasing drag and possible flow separation, which can reduce overall turbine efficiency and increase unsteady loading.

These insights can be integrated into blade element momentum (BEM) analyses or system-level simulations to estimate turbine power output and to design pitch or control strategies for optimal performance.

IV. CONCLUSION

This paper has presented a CFD analysis of an airfoil at low angles of attack using a structured MultiZone mesh in ANSYS. The main findings can be summarized as follows:

1. A high-quality mesh with approximately 540,000 elements and maximum skewness below 0.26 was successfully generated around the airfoil, providing a reliable basis for CFD simulations.
2. Steady-state simulations at −5°, 0°, 5°, and 10° angles of attack show physically consistent trends in pressure and velocity fields, including attached flow at low angles and increasing wake thickness at higher angles.
3. Lift increases with angle of attack, while drag also rises, resulting in an optimal operating region around a moderate angle (approximately 5°) where the lift-to-drag ratio is favorable.
4. The results provide useful preliminary guidance for the selection of airfoil operating angles in small-scale wind turbine blade design and lay the groundwork for future studies that may include additional Reynolds numbers, turbulence models, and stall behavior.

Future work will focus on refining the boundary-layer resolution, extending the angle-of-attack range into deep stall, and coupling the present aerodynamic results with turbine-level performance calculations.

V. REFERENCES

B. Wei, etal "A novel wall interference correction method for airfoil," *Adv. Aerodyn.*, pp. 1–21, 2024, doi: 10.1186/s42774-024-00193-1.

J. P. Narayanan, et al, "A Framework to Generate Shape Optimised Profiles for a Cambered Airfoil Approaching Ground," *Iran. J. Sci. Technol. Trans. Mech. Eng.*, vol. 49, no. 1, pp. 499–516, 2025, doi: 10.1007/s40997-024-00824-4.

K. S. Bhole, et al "Computational analysis of a new airfoil for micro-capacity wind turbine," *Int. J. Interact. Des. Manuf.*, 2023, doi: 10.1007/s12008-023-01419-0.

M. A. Aziz, etal "Multi-slotted airfoil design for enhanced aerodynamic performance and economic efficiency," pp. 1–18, 2025.

S. M. T. Islam, et al, "A Novel Prediction Model for Airfoil Aerodynamic Characteristics Based on Machine Learning," *Iran. J. Sci. Technol. Trans. Mech. Eng.*, vol. 49, no. 3, pp. 1249–1267, 2025, doi: 10.1007/s40997-025-00850-w.

V. Filipe, etal "Exergy - based assessment of airfoil drag," *J. Brazilian Soc. Mech. Sci. Eng.*, vol. 47, no. 5, pp. 1–23, 2025, doi: 10.1007/s40430-025-05506-z.

W. Du *et al.*, "The effects of surface modification on aerodynamic characteristics of airfoil," *Int. J. Thermofluids*, vol. 16, no. Septem

Y. T. Lee, K. Ramesh, and A. Gopalarathnam, *Effect of rounded trailing edges on unsteady airfoil loading at low reynolds numbers*, vol. 0123456789. Springer Berlin Heidelberg, 202